Oxygen and sulfur stable isotope ratios of Late Devonian vertebrates trace the relative salinity of their aquatic environments

Jean Goedert, David Broussard, Jeffrey Trop, Edward Daeschler, Romain Amiot, François Fourel, Sébastien Olive, Arnauld Vinçon-Laugier, Christophe Lécuyer

▶ **To cite this version:**

Jean Goedert, David Broussard, Jeffrey Trop, Edward Daeschler, Romain Amiot, et al.. Oxygen and sulfur stable isotope ratios of Late Devonian vertebrates trace the relative salinity of their aquatic environments. Geological Society of America Bulletin, 2024, 10.1130/B37631.1 . hal-04769137

HAL Id: hal-04769137
https://hal.science/hal-04769137v1

Submitted on 15 Nov 2024

HAL is a multi-disciplinary open access archive for the deposit and dissemination of scientific research documents, whether they are published or not. The documents may come from teaching and research institutions in France or abroad, or from public or private research centers.

L'archive ouverte pluridisciplinaire **HAL**, est destinée au dépôt et à la diffusion de documents scientifiques de niveau recherche, publiés ou non, émanant des établissements d'enseignement et de recherche français ou étrangers, des laboratoires publics ou privés.

Oxygen and sulfur stable isotope ratios of Late Devonian vertebrates trace the relative salinity of their aquatic environment

Goedert Jean[1], Broussard David[2,*], Trop Jeffrey[3], Daeschler Edward[4], Amiot Romain[5], Fourel François[6], Olive Sébastien[5, 7, 8], Vinçon-Laugier Arnauld[5] and Lécuyer Christophe[5]

[1]*Muséum National d'Histoire Naturelle, Centre de Recherche en Paléontologie – Paris (CR2P), CNRS/MNHN/Sorbonne Université, CP 38, 57 rue Cuvier, F–75231 Paris cedex 05, France.*

[2]*Department of Biology, Lycoming College, Williamsport, PA, 17701, U.S.A.*

[3]*Department of Geology and Environmental Geosciences, Bucknell University, Lewisburg, PA, 17889, U.S.A.*

[4]*Academy of Natural Sciences of Drexel University, 1900 Benjamin Franklin Parkway, Philadelphia, PA, 19118, U.S.A.*

[5]*Universite Claude Bernard Lyon 1, CNRS, ENSL, UJM, LGL-TPE, UMR 5276, Villeurbanne, F-69100.*

[6]*Universite Claude Bernard Lyon 1, CNRS, ENTPE, LEHNA, UMR 5023, Villeurbanne, F-69100.*

[7]*Royal Belgian Institute of Natural Sciences, Directorate Earth and History of Life, Palaeobiosphere Evolution, Rue Vautier 29, 1000 Brussels, Belgium.*

[8]*Université de Liège Freshwater and Oceanic Science Unit of Research Laboratory of Ecology and Conservation of Amphibians, Quai Van Beneden, 22, 4020 Liège, Belgium.*

*jean.goedert@protonmail.com; *broussar@lycoming.edu (corresponding author); jtrop@bucknell.edu; ebd29@drexel.edu; romain.amiot@univ-lyon1.fr; francois.fourel@univ-lyon1.fr; solive@naturalsciences.be; arnauld.vincon-laugier@univ-lyon1.fr; christophe.lecuyer@univ-lyon1.fr*

ABSTRACT

Late Devonian aquatic environments hosted the fin-to-limb transition in vertebrates. Upper Devonian (365 – 360 Ma) strata in Pennsylvania, USA, preserve a diversity of fishes and tetrapods in coastal marine to fluvial depositional environments, making this region ideal for investigating the ecology and evolution of Late Devonian vertebrates. A key unresolved issue has been reconstructing the specific aquatic habitats that hosted various vertebrates during this period. Specifically, the salinity of environments spanning fresh to shallow marine water is difficult to discern from sedimentological and paleontological analyses alone. Here, we analyze Rare Earth Elements and Yttrium as well as stable oxygen and sulfur isotope compositions ($\delta^{18}O$, $\delta^{34}S$) in fossil vertebrate bioapatite from the Catskill and Lock Haven formations in the Appalachian Basin, USA, to determine the relative salinity of their aquatic environments. These results confirm the ecological euryhalinity of several taxa (*Bothriolepis* sp., tristichopterids and *Holoptychius* sp.). The results also confirm that early tetrapod species found to date in the Catskill Formation lived mainly in freshwater aquatic environments. Our study shows that integrating sedimentological and paleontological data with combined oxygen and sulfur isotope analysis allows precise tracing of the relative salinity of vertebrate habitats deep in the past.

Keywords: Stable isotope geochemistry; Rare Earth Elements; Early tetrapods; Aquatic paleoecology; Famennian; Sedimentology

INTRODUCTION

During the Late Devonian Period (385 – 360 Ma) the continued development of terrestrial ecosystems and the diversification of vertebrates took place, including the rise of early tetrapods (Clack, 2002), from which originated modern amphibians, reptiles and mammals. Coastal paleoenvironments with variable salinities including estuaries and tidally-influenced rivers have been identified as important habitats that hosted vertebrate evolution during this time (Sallan et al., 2018; Byrne et al., 2020; Gess and Whitfield, 2020).

Modern transitional aquatic environments evolve between freshwater (in most cases river water < 0.5 ppt) and saline environments (0.5 ppt to 30 ppt for brackish waters; marine waters from 30 to 40 ppt with an average present-day value of 34.5 ppt). They are characterized by salinity gradients that define and structure many habitats for aquatic organisms (Young et al., 2018; Zhang et al., 2021). The shifting spatial and temporal boundaries of these habitats are further complicated as salinity gradients are not only horizontal but also vertical, and as these change with tidal and seasonal cycles, or with extreme episodic events such as storms or floods (Geawhari et al., 2014; Veale et al., 2014; Cloern et al., 2017; Xia et al., 2017). Many extant fish species are euryhaline in that they are able to tolerate varying salinities (e.g., Zydlewski and Wilkie 2012; Every et al., 2017; Colombano et al., 2020). Some other species occupy aquatic environments of different salinities during their lifetime (i.e., migratory species; Rountree and Able 2007). They may migrate from one habitat to another cyclically (tidal, diel, seasonal or other repeated cycles) or ontogenically (i.e., physiological euryhalinity cf. Schultz and McCormick (2012)). These different habitats serve different functions among which include nutrition, reproduction, and protection from predators (Rountree and Able 2007). Within the same species, different populations can also inhabit aquatic environments of different salinities without changing during their lifetime (i.e. ecological euryhalinity cf. Schultz and McCormick (2012)).

Stable isotopes, particularly those of sulfur in dissolved sulfates in aquatic environments, are accurate tracers of mixing processes between fresh and marine waters in transitional environments such as estuaries (Peterson 1986; Fry 2002a). Numerous studies demonstrate that sulfur isotope composition analysis is a particularly suitable tool for characterizing the aquatic habitats of fish species (Hesslein et al. 1991; Fry 2002b; Dubé et al., 2005; Fry and Chumchal 2011; Trembaczowski 2011; Nehlich et al., 2013; Carr et al., 2017; Pizzochero et al., 2017). Sulfur isotopes, for example, help to distinguish within the same river system and

within the same fish population, sedentary individuals from those making downstream migrations (Carr et al., 2017) to estuarine and marine areas (Hesslein et al., 1991; Fry and Chumchal 2011). Sulfur isotope analysis of fish otoliths also reflects the variation in the salinity of their aquatic habitats (Weber et al., 2002; Godebout et al., 2010, 2011; Doubleday et al., 2018).

In the Late Devonian Period, a key unresolved issue has been reconstructing the specific aquatic habitats that hosted various vertebrates including early tetrapods. Specifically, the salinity of environments spanning fresh to shallow marine water is difficult to discern from sedimentological and paleontological analyses alone. Euryhaline adaptations may have played a key role in the Paleozoic colonization of continental freshwater ecospaces by vertebrates (e.g., Cloutier et al., 2011; Carpenter et al., 2015; Gogáin et al., 2016; Goedert et al., 2018; Gess and Whitfield 2020). However, the lack of high-resolution paleosalinity proxies from sedimentological and paleontological analyses has hampered efforts to evaluate the impact of salinity gradients in vertebrate evolution, including the fin-to-limb transition.

Goedert et al. (2016) demonstrated that the sulfur isotope composition of apatite from present-day and fossil vertebrates could be accurately measured and that these reflect the sulfur isotope composition of the sulfates in their aquatic environments (Goedert et al., 2018; 2020; 2023). They further demonstrated the potential of the combined oxygen and sulfur isotope analysis to trace the relative salinity of aquatic environments, and showed that some early tetrapods and their associated vertebrate species from the Late Devonian of Eastern Greenland and China lived in aquatic environments subject to marine influence (Goedert et al., 2018). Nevertheless, the samples analyzed in that study lacked precise stratigraphic provenance and were therefore not associated with a precisely identified depositional setting, which limited interpretation of the results. Notably, such sampling collection did not allow testing whether or not the combined oxygen and sulfur isotope analysis has the potential to highlight more subtle differences in salinity that should characterize more or less proximal/distal localities.

Upper Devonian (Famennian, 365 – 360 Ma) strata in Pennsylvania, USA, preserve especially abundant and diverse vertebrates, including early tetrapods, in fluvial to coastal marine depositional environments, making this region ideal for investigating ecological aspects associated with the fin-to-limb transition (Cressler et al., 2010; Broussard et al., 2018, 2020). This study demonstrates a “proof of concept” combined stable isotope (oxygen and sulfur) methodology on Famennian vertebrate fossils from four localities (Fig. 1A-D;

Supplementary Material Item (SMI) 1) spanning fluvial, transitional and shallow-marine environments across a 60 km-long transect. We compare the relative salinities of the aquatic habitats frequented by these vertebrates inferred from isotopic data to those of their depositional environments deduced from sedimentological and paleontological data to better understand the ecologies of these Late Devonian aquatic faunas.

GEOLOGIC SETTING

Devonian siliciclastic sedimentary strata accumulated in the northern Appalachian foreland basin inboard (west, modern coordinates) of a convergent plate margin at tropical to subtropical paleolatitudes (Fig. 1C; Blakey 2008). Plate convergence prompted westward (modern coordinates) migration of the fold-thrust belt and westward progradation of alluvial-fluvial depositional systems into a shallow epicontinental seaway (Ver Straeten et al., 2010). As a result, the Upper Devonian stratigraphy of north-central Pennsylvania consists of > 3 km-thick succession of siliciclastic sedimentary strata (Slingerland et al., 2009). The Lock Haven Formation reflects deposition in shallow marine environments (Castle 2000; Beard et al., 2017), whereas the overlying Catskill Formation records deposition mainly in fluvial and coastal plain environments (Daeschler and Cressler 2011; Broussard et al., 2018; 2020). Broad open folds deform these strata as a result of post-depositional crustal shortening (~13 % along the sampled transect; Sak et al., 2012).

MATERIAL AND METHODS

Sampling strategy

Famennian vertebrate taxa were sampled from four outcrops: Steam Valley (SV), Blossburg (Bl) and Tioga (Ti) representing the Catskill Formation and Covington (Co) Middle (CoM) and South (CoS) representing the Lock Haven Formation (Fig. 1; SMI 1, 2). Sampled strata accumulated in fluvial (SV), transitional marine-fluvial (Bl and Ti), and coastal shallow marine (Co) environments, based on previously published sedimentological and paleontological data (SMI 1). The Catskill and Lock Haven formations strata contain several vertebrate genera of “placoderms”, “acanthodians”, and osteichthyans including early tetrapods (SMI 3; Cressler et al., 2010; Broussard et al., 2020). Additionally, these strata preserve fossil floras and

invertebrates, providing insight into marine and fluvial ecosystems and environments. Qualitative interpretations of paleosalinity for the depositional settings of the sampled outcrops are based on position within the gradient from alluvial plain to marine lithofacies associations (SMI 1).

For each locality, 10 specimens of fossil vertebrate taxa were sampled (SMI 4–7) and processed for oxygen and sulfur stable isotopic analyses (SMI 8) and for elemental analyses (SMI 9) including Rare Earth Element and Yttrium (REY; SMI 10). Sampled taxa include "placoderms" (*Bothriolepis* sp., a single *Phyllolepis* sp. from Bl locality and pachyosteomorph arthrodires from Co localities) and sarcopterygians (a single Dipnoi indet., *Holoptychius* sp., *Eusthenodon bourdonii* and *Langlieria radiatus*). *Bothriolepis*, *Phyllolepis*, and sarcopterygians were sampled from Catskill Formation outcrops interpreted as fluvial and transitional environments (SV, Bl, and Ti) whereas pachyosteomorph arthrodires were sampled from Lock Haven Formation outcrops interpreted as coastal shallow marine environments (CoS and CoM; SMI 11–13).

Biogenic apatite sampling

Biogenic apatite (bones, scales and teeth, SMI 8) powders were sampled by using a spherical diamond tip drill bit or by crushing small fragments in an agate mill. Potential trace of sediments or diagenetic minerals were removed using thin needles under binocular microscope. The specimen was beforehand cleaned using acetone to remove potential traces of glue on the surface. Then, for each sample, the outermost apatite layer is removed before sampling to avoid potential surface sediment contamination. Each bioapatite powder sample was subdivided into three aliquots of 3 mg, 20 mg and 0.7 mg for oxygen isotope analysis of bioapatite phosphate, sulfur isotope analysis of bioapatite, and elemental analysis, respectively. For each locality, a sediment sample associated with a fossil apatite (SV-6; Bl-1; Ti-1 and CoM-9; SMI 9 and 10) was also collected in powder form using a spherical diamond tip drill bit.

Elemental analysis

Concentrations of major and trace elements were measured respectively on an inductively coupled plasma atomic emission spectrometer (ICP-AES; ICAP 7400 Series, Thermo Scientific) and on an inductively coupled plasma mass spectrometer (ICP-MS; ICAP-Q, Thermo Scientific). The reliability of measurements has been controlled through a set of blanks and the reference material NIST-SRM1486. Before measurements,

approximately 0.7 mg of each sample (scale, bone, tooth or sediment) was dissolved in 2 mL of distilled 14 M nitric acid at 150 °C for 48 hours (SMI 9 and 10).

Oxygen isotope analysis of bioapatite phosphate

Each 3 mg apatite powder aliquot was pre-treated according to the wet chemistry protocol initially described by Crowson et al. (1991), and subsequently modified by Lécuyer et al. (1993) and then adapted by Bernard et al. (2009) for small sample weights (3 mg). For samples from Co localities, a quantity of apatite powder > 3 mg was collected for oxygen isotope analysis and these samples were pre-treated using the standard protocol (Lécuyer et al. 1993). This protocol involves the isolation of phosphates (PO_4^{3-}) from bioapatite as silver phosphate (Ag_3PO_4) crystals using acid dissolution and anion-exchange resin. For each sample, enamel powder was dissolved in 1 mL of 2 M HF overnight. The CaF_2 residue was separated in a centrifuge and the solution neutralized by adding 1 mL of 2 M KOH. Amberlite anion-exchange resin (1.5 mL) was added to the solution to separate the PO_4^{3-} ions. After 4 h, the solution was removed and the resin was eluted with 6 mL of 0.5 M NH_4NO_3. After 4 h, 0.1 mL of NH_4OH and 3 mL of an ammoniacal solution of $AgNO_3$ were added and the samples were placed in a thermostated bath at 70 °C for 6 h, enabling the precipitation of Ag_3PO_4 crystals. Oxygen isotope compositions were measured at the Laboratoire d'Écologie des Hydrosystèmes Naturels et Anthropisés (LEHNA) in Lyon and at the Laboratoire de Géologie de Lyon using a high-temperature pyrolysis technique involving a Vario PYRO cube™ elemental analyzer interfaced in continuous flow mode to an Isoprime or a Precision™ isotope ratio mass spectrometer (the EA-Py-CF-IRMS technique; Lécuyer et al., 2007; Fourel et al., 2011). For each sample, 5 aliquots of 300 µg of Ag_3PO_4 were mixed with 300 µg of pure graphite powder and loaded in silver foil capsules. Pyrolysis was performed at 1450 °C. Measurements were calibrated against NBS120c ($\delta^{18}O$ = + 21.7 ‰ V-SMOW; Lécuyer et al., 1993) and a homemade standard CAL-3 (silver phosphate, Ag_3PO_4: $\delta^{18}O$ = + 5.46 ‰ V-SMOW; Lécuyer et al., 2019). Silver phosphate samples precipitated from standard NBS120c were repeatedly analyzed ($\delta^{18}O$ = + 21.7 ‰; 1σ = 0.4 ‰; n = 16) along with the silver phosphate samples derived from fossil bioapatites to ensure that no isotopic fractionation occurred during the wet chemistry. The average standard deviation was 0.2 ± 0.1 ‰. Data are reported as $\delta^{18}O_p$ values in "‰" relative to the V-SMOW scale. The official international unit to report isotopic ratio is the Urey (Ur). As it is a more common practice we have reported isotopic data in "‰" units with 1 ‰ = 1 mUr.

Sulfur isotope analysis of bioapatite

Sulfur isotope compositions were measured using a Vario PYRO cube™ elemental analyzer in NCS combustion mode interfaced in continuous-flow mode with an Isoprime100™ isotope ratio mass spectrometer hosted at the LEHNA. For each bioapatite sample, 3 aliquots of 7 mg of bioapatite powder were mixed with around 20 mg of tungsten oxide (WO_3) powder and loaded in tin foil capsules. Tungsten oxide is a powerful oxidant ensuring the full thermal decomposition of bioapatite sulfate into sulfur dioxide (SO_2) gas (Goedert et al., 2016). Measurements have been calibrated against the IAEA-S-2 (silver sulfide, Ag_2S $\delta^{34}S$ = + 22.62 ‰ (V-CDT); Halas and Szaran 2001), IAEA-SO-5 (barium sulfate, $BaSO_4$ $\delta^{34}S$ = + 0.5 ‰ (V-CDT); Halas and Szaran 2001) and IAEA-SO-6 (barium sulfate, $BaSO_4$ $\delta^{34}S$ = - 34.1 ‰ (V-CDT); Halas and Szaran 2001) international standards. For each analytical run of bioapatite samples, we have also analyzed BCR32 samples as a compositional (S % = 0.72, certified value; Community Bureau of Reference 1982) and isotopic standard ($\delta^{34}S$ = + 18.4 ‰ (V-CDT); Fourel et al. 2015; Goedert et al. 2016) to ensure that analytical conditions were optimal to perform sulfur isotope analyses of samples with low-S content (we measured BCR32 over four analytical sessions: $\delta^{34}S$ = + 18.8 ‰ ± 0.3 ‰ (1σ) and S content = 0.76 % ± 0.03 % (1σ); n = 4). 5 aliquots (270 µg each) of IAEA-S2 were systematically analyzed at the beginning and end of each analytical batch to correct for potential instrumental drift effects. Smaller aliquots of IAEA-S2 weighing 90 µg have also been analyzed allowing to correct possible isotopic fractionation of instrumental origin for samples with low intensity (around 1 nA). It is worth noticing that samples SV-5 and T-4 have been analyzed in two different analytical sessions (each time three aliquots) and delivered statistically identical values (+10.0‰ ± 0.07 ‰ *vs* +10.1‰ ±0.18‰ and +16.0‰ ±0.49‰ *vs* +16.1‰ ± 0.08‰, respectively). The sample average standard deviation for $\delta^{34}S$ measurements is 0.2 ‰ ± 0.2 ‰. Data are reported as $\delta^{34}S$ values in "‰" relative to the V-CDT scale. The official international unit to report isotopic ratio is the Urey (Ur). As it is a more common practice we have reported isotopic data in "‰" units with 1 ‰ = 1mUr.

RESULTS AND DISCUSSION

Taphonomy

Fossil specimens were collected from disarticulated individuals and exhibit various degrees of abrasion and fragmentation (SMI 14). Fossil samples from Ti and Co show the highest degree of abrasion and fragmentation, indicative of substantial post-mortem transport. Samples from fluvial strata (Bl and SV) show medium to low levels of abrasion and fragmentation indicating less post-mortem transport of specimens compared to those from transitional and shallow marine strata (Ti and Co, respectively; Broussard et al., 2020).

Rare Earth and Yttrium elements

Rare Earth and Yttrium (REY) elements are incorporated post-mortem into bioapatites primarily during early diagenesis from pore waters (Trueman and Tuross 2002; Trotter et al., 2016). Thus, fossil bioapatites acquire REY concentrations characteristic of the diagenetic environment and can be useful for disentangling potential different diagenetic histories within a fossil assemblage (Trueman and Tuross 2002).

Most of the fossil apatite samples analyzed here have $(La/Sm)_N$ ratios < 0.3 (Fig. 2; SMI 10). This implies that these fossil bioapatites probably underwent at least one later phase of diagenetic incorporation of REY *via* substitutional mechanisms leading to enrichment in Medium Rare Earth Elements (MREE; Reynard et al., 1999). Interestingly, sedimentary samples from SV, Bl and Ti have $(La/Sm)_N$ ratios > 0.3, that fall within the domains characterizing modern fresh to coastal waters and range along this salinity gradient in perfect coherence with their characterization in terms of depositional environment; Ti locality being considered more distal than Bl, itself more distal than SV (Broussard et al., 2020). Most Ti samples also have $(La/Sm)_N$ ratios > 0.3, suggesting that they have retained their primary diagenetic signature. By applying the partition coefficients between apatite and water (Koeppenkastrop and De Carlo 1992) we calculated the REY concentrations of the pore waters from which they acquired this signature (Trotter et al., 2016). Interestingly, these show $(La/Sm)_N$ and $(La/Yb)_N$ ratios compatible with those of modern transitional aquatic environments (Fig. 2); this is again in agreement with a fluvial-marine transitional environment interpreted for Ti from sedimentological data (Slane et al., 2009; Broussard et al., 2020).

Fossil bioapatites record REY patterns that are highly consistent within a single locality, but differ between localities. The Ti locality, for example, shows marked differences from the others, notably expressed by the presence of three negative anomalies in europium (Eu), terbium (Tb) and yttrium (Y) and a more moderate enrichment in MREE. The SV and Bl localities show very similar patterns suggesting similar fossilization environments, which is again consistent with an interpretation in terms of similar depositional environments for these two localities, Bl being more distal than SV locality. The Co localities also show similar REY profiles, but is nevertheless distinguished from SV and Bl localities by a negative neodymium (Nd) anomaly (Fig. 2).

It is particularly interesting to note that within the Ti locality, sample Ti-8 shows a REY profile different from the other samples, with a marked enrichment in MREE. In fact, this sample shows a pattern very similar to the Bl and SV localities. Its $\delta^{18}O_p$ and $\delta^{34}S$ values are also close to those from the Ti locality (Fig. 3). These observations strongly suggest that this sample has been reworked, potentially from a locality further upstream in the sedimentary depositional system, which is again consistent with a more proximal depositional environment for the SV and Bl localities compared with Ti, which is interpreted as more distal.

Evaluation of primary preservation of stable isotope compositions

Post-mortem, bioapatite mineral that composes the skeleton can be modified during diagenesis (e.g., Keenan et al., 2015; Keenan 2016; Keenan and Engel 2017). The original content of one or more elements can be altered as well as its pristine isotopic compositions but not in a systematic and *a priori* predictable way, which implies to evaluate each element separately when assessing diagenesis (e.g., Sponheimer and Lee-Thorp 2006; Martin et al., 2018).

Unlike the oxygen isotope composition of carbonate, the oxygen isotope composition of bioapatite phosphate is more robust regarding diagenetic alteration (e.g., Shemesh et al., 1983; Lécuyer et al., 1999). For each locality, there is no significant correlation between phosphate $\delta^{18}O_p$ values and its concentration in the bioapatite (SMI 15). Moreover, 95% of Ca/P ratio values are within the modern variability ($1.99 \leq Ca/P \leq 2.33$; Legeros et al., 1984). These two observations indicate dissolution-recrystallization processes that occurred during early diagenesis did not involve a substantial replacement of the pristine phosphate component by exogenous sources of phosphate with different oxygen isotope compositions.

The sulfur isotope composition of sulfate that substitutes to phosphate in bioapatite can be overprinted by the addition of diagenetic mineral such as iron sulfide, which can have a very low sulfur isotope composition (e.g., Goedert et al. 2023). Following this assumption, if bioapatite samples were contaminated by diagenetic sulfide minerals, we would therefore expect to observe a positive correlation between $\delta^{34}S$ values and the inverse of sulfur concentration (SMI 15). Here, no significant correlations are observed for neither the Bl, Ti nor Co localities (SMI 15). However, two samples (CoM-1 and CoM-2) have negative $\delta^{34}S$ values (SMI 8). Although these values are not incompatible with those of freshwater environments (Nehlich 2015) (and the sulfur concentration of these samples (< 1 %) is not incompatible with *in vivo* concentrations either) we cannot rule out slight contamination of the bioapatite by a sulfide source with very negative $\delta^{34}S$ values. We will therefore treat these two samples with caution in the following interpretations. Additionally, it is worth noting that the average sulfur concentrations of the samples (either by AES or by the elemental analyzer TCD system) are all less than 1% (except for CoM-3, CoM-7 and CoM-8) and relatively homogeneous (average S content equals 0.22 ± 0.11% by TCD and 0.39 ± 0.22% by AES). Such values are rather compatible with the expected biogenic concentrations in vertebrate bioapatite.

Eventually, we do not observe any significant correlations between the isotopic compositions of oxygen or sulfur and the concentrations of elements typically incorporated in bioapatite during diagenesis, such as REY, manganese, iron, thorium and uranium (SMI 9 and 10). All these considerations lead us to assume that these Devonian bioapatite samples have retained at least part of their pristine oxygen and sulfur isotopic compositions, which can be used to make paleoenvironmental inferences.

Oxygen and sulfur isotopes

The oxygen isotope composition of marine waters ranges generally from - 2‰ to + 2 ‰, and in most cases is ^{18}O-enriched relative to freshwater, except for freshwater from dry tropical environments (Dansgaard 1964; Craig and Gordon 1965; Rozanski et al., 1993). Concerning sulfur isotope composition, marine environments generally have $\delta^{34}S$ values of dissolved sulfates higher than freshwater ones, close to +21 ‰ for modern marine environments (Nehlich 2015; Goedert et al. 2020). Knowing that the isotopic fractionation between the sulfur of apatite and that of sulfates in aquatic environments is close to 0 ‰ (Goedert et al., 2018), the sulfur isotopic composition of apatites directly reflects that of the dissolved sulfates of aquatic

276 environments in which the sampled vertebrates lived. However, to date, there are no published data of $\delta^{34}S$
277 values of vertebrates from typical and exclusive Devonian marine species (e.g., conodont) to compare with.
278 Nonetheless, the sulfur isotopic composition of marine environments can also be traced through that of marine
279 carbonates that also reflects directly that of the sulfates of marine waters. Several studies have measured
280 elevated $\delta^{34}S$ values of marine carbonates ranging from + 20 to + 30 ‰ during the Famennian (Kampschulte
281 and Strauss 2004; Peryt et al., 2007; Sim et al., 2015; Paytan et al., 2020).

282 The 40 analyzed Devonian vertebrate samples have $\delta^{18}O_p$ values ranging from + 11.5 ‰ to + 14.9 ‰
283 (Fig. 3; SMI 8). Average $\delta^{18}O_p$ values of vertebrates from SV and Bl do not differ significantly ($\delta^{18}O_p$ = + 13.0 ‰ ±
284 0.6 ‰ (n = 10) *vs* $\delta^{18}O_p$ = + 13.2 ‰ ± 0.3 ‰ (n = 10); Mann-Whitney test: p-value = 0.2863). However, average
285 $\delta^{18}O_p$ values from Ti and from CoM are respectively and significantly higher ($\delta^{18}O_p$ = + 14.1 ‰ ± 0.8 ‰ (n = 10))
286 and lower ($\delta^{18}O_p$ = + 12.0 ‰ ± 0.3 ‰ (n = 9)) than those from SV and Bl (Cf. Mann-Whitney pairwise test in SMI
287 16). There are no systematic differences in the $\delta^{18}O_p$ values of different taxa (i.e., *Bothriolepis* sp., *Holoptychius*
288 sp., *E. bourdonii*) between the different localities.

289 With regard to sulfur, the 40 analyzed Devonian vertebrate samples have $\delta^{34}S$ values ranging from +
290 6.0 ‰ to + 20.7 ‰ (without considering the two negative values; see explanations above; Fig. 3; SMI 8). SV, Bl,
291 Ti and CoM have average $\delta^{34}S$ values of + 10.0 ‰ ± 2.5 ‰ (n = 10), + 17.1 ‰ ± 1.4 ‰ (n = 9), + 14.5 ‰ ± 2.1 ‰
292 (n = 10) and + 8.5 ‰ ± 1.8 ‰ (n = 4), respectively. All these values are significantly different from each other
293 (except between SV and CoM cf. Mann-Whitney pairwise test in SMI 16). The localities of SV and Ti show
294 systematic differences in $\delta^{34}S$ values between different taxa. At SV, for instance, the sulfur isotope values vary
295 systematically among the different taxa (+ 6.8 ‰ to + 8.1 ‰ in *Bothriolepis* sp., + 9 ‰ to + 10.5 ‰ in
296 *Holoptychius* sp., + 10.1 ‰ to + 13.8 ‰ in *E. bourdonii*). These preliminary results, suggest that subtle changes
297 in the relative salinity play an important role in the structuring of aquatic ecosystems, as currently the case in
298 modern ones and as has been highlighted for other Upper Devonian taxa (Goedert et al. 2018). The lower $\delta^{34}S$
299 values of *Bothriolepis* sp. could also reflect a benthophagous lifestyle as observed for some modern vertebrate
300 taxa (Croisetière et al., 2009; De Brabandere et al., 2009; Ponton and Hare 2015; Goedert et al., 2020;), which
301 would fit well with the benthophagous lifestyle proposed independently for this taxon from its anatomical
302 study (e.g., Béchard et al., 2014; Chevrinais et al., 2017). However, these observations are only based on a

small number of individuals per taxon and would deserve further investigation to provide appropriate statistical support.

Devonian bioapatite samples from SV, the most proximal locality, have low $\delta^{18}O_p$ and $\delta^{34}S$ values consistent with freshwater aquatic environments. The significantly higher $\delta^{34}S$ values of Bl and Ti (SMI 16) are indicative of marine influence, in agreement with their distal position compared to SV (Broussard et al., 2020). Nonetheless, they are still not compatible with strictly marine environments during Late Devonian time. $\delta^{18}O_p$ values of Devonian bioapatite sampled from shallow marine and transitional environments (Co and Ti sites, respectively) are substantially lower (even the highest value, i.e., + 14.9 ‰) than those reported from strictly marine organisms, such as conodonts, that typically yield $\delta^{18}O_p$ values ranging from + 16.5 ‰ to + 19 ‰ during Late Devonian time (Joachimski et al., 2009; Chen et al., 2021). While these differences may reflect the relatively shallow coastal conditions of the sample sites, they may also be a product of the epicontinental setting that characterized the studied region during Late Devonian time with shallow coastal water mass potentially diluted locally by freshwater inputs from orogenic sources (Acadian orogeny) (Fig. 1; Gilleaudeau et al., 2021).

The vertebrate sample from the CoS locality has the highest $\delta^{34}S$ value of the entire dataset ($\delta^{34}S$ = + 20.7 ‰), compatible with $\delta^{34}S$ values of marine environments at that time (Goedert et al., 2018). Its $\delta^{18}O_p$ value, on the other hand, is low for typical marine values. This can be explained by the dilution effect cited above that affects more oxygen isotopic composition since oxygen is more sensitive than sulfur to mixing process with freshwater (Goedert et al. 2018). Vertebrate samples from the CoM locality have the lowest $\delta^{18}O_p$ and $\delta^{34}S$ values, which are clearly incompatible with those of Late Devonian marine environments. The fossiliferous horizon at CoM contains a mix of marine (brachiopods, crinoids, ctenacanthids, and *Orodus* sp.) and freshwater fauna (lungfish). Moreover, the CoM vertebrate fossil horizon is a rare red sandstone unlike surrounding grey strata that bear sedimentary structures diagnostic of wave- and tidal- processes (SMI 12). Given the sedimentology, taphonomy, and stable isotope values of the pachyosteomorph samples, it is likely that they originated in freshwater, upstream environments and were transported post-mortem and deposited into shallow marine environments preserved at the CoM locality. Previously, isolated remains of pachyosteomorphs have been identified from fluvial strata at the Ti and Bl localities (Broussard et al., 2022). Considering these occurrences and our stable isotope data together, large pachyosteomorph arthrodires (ca. 5

– 7 m in length) were likely able to tolerate a range of environments based on salinity and were not restricted to marine environments in the Late Devonian northern Appalachian Basin (Carr 2010).

Apatites from the Ti locality have slightly lower $\delta^{34}S$ values than those from Bl, which is considered to have been more proximal compared to Ti (Broussard et al., 2020). Similar to the CoM "placoderm" samples, this may be explained by post-mortem transport of the Ti assemblage fossils from lower salinity upstream environments, as indicated by their high degree of abrasion and fragmentation (SMI 14).

Paleoecological inference

Taken together, oxygen and sulfur isotope compositions confirm previously reported sedimentological data that many Late Devonian vertebrate species are euryhaline (at least ecologically), living in aquatic environments ranging from fluvial, transitional fluvial-coastal plain, and shallow marine environments. Isotopic data clearly reveal the influence of water of higher salinity for the locality of Bl and CoS (higher $\delta^{34}S$ values) and for the locality of Ti (both higher $\delta^{18}O_p$ and $\delta^{34}S$ values), which is compatible with depositional models (Fig. 1; SMI 2; Slane et al., 2009; Broussard et al., 2018, 2020).

Although oxygen isotope values are rather comparable with those measured in Late Devonian vertebrate bioapatites of Eastern Greenland and China, sulfur isotope compositions from Greenland and China yield significantly higher values (> + 20 ‰; Goedert et al., 2018) than the Appalachian vertebrates reported herein (Fig. 4). This difference may be explained by the China and Greenland vertebrates inhabiting more seaward habitats although the paleoenvironment of the China and Greenland samples (Goedert et al., 2018) is not well constrained.

The different ecosystems represented by these aquatic environments with varying degrees of salinity supported a diverse array of vertebrate taxa including sarcopterygians and early tetrapods within the fin-to-limb transition. Previous work at other locations globally have reported early tetrapod remains from transitional environments (e.g., Goedert et al., 2018; Gess and Whitfield 2020). However, no early tetrapods have been reported from Upper Devonian strata interpreted as transitional or shallow marine environments anywhere in the Appalachian basin. To date, in the Appalachian basin early tetrapod remains have been collected from the SV locality alongside taxa sampled in this analysis (Downs et al., 2021). In addition, they have been reported from Famennian strata at the Red Hill and Trout Run sites (not part of this study), which are

358 interpreted as freshwater depositional environments based on sedimentological and paleontological data (Fig.
359 1D; Daeschler et al., 2009; Broussard et al., 2018). Thus, isotopic data reported herein support previous
360 sedimentological data that indicate Late Devonian tetrapods inhabited fluvial environments in the Appalachian
361 basin.

362

Conclusions

Integration of geochemical data with sedimentological and paleontological data allow for robust reconstruction of vertebrate habitats deep in the past. Our study is the first to assess relative paleosalinity of Late Devonian aquatic ecosystems in the Appalachian Basin via integrated geochemical, sedimentological, and paleontological data. Using this novel approach, we show that oxygen and sulfur isotope compositions of Devonian vertebrate bioapatites reflect the relative salinity differences between SV, Bl, Ti and CoS localities in agreement with sedimentological interpretations, with the exception of the CoM locality. Fossil vertebrate samples from the CoM locality have isotopic values clearly compatible with freshwater environments that differ from sedimentary and paleontological data that indicate a coastal shallow marine depositional environment. Taphonomic data (i.e., degree of abrasion) and REY patterns suggest that CoM vertebrate remains were transported from upstream, freshwater environments. This underlines the importance of distinguishing between depositional and living environments when interpreting isotopic data to make paleoecological inferences. Overall, these new geochemical data are consistent with previous environmental affiliations of sampled taxa derived from sedimentological and paleontological observations. These geochemical results confirm the ecological euryhalinity of several Late Devonian vertebrate taxa. A majority of Late Devonian early tetrapod body fossils originate from aquatic environments subjected to marine influence (Olive et al., 2016; Goedert et al., 2018; Gess and Whitfield 2020). Our results are the first demonstrating that some early tetrapod species occupied unequivocally freshwater habitats by ca. 362-360 Ma. The analytical techniques employed in our study should be of special concern to those workers interested in assessing the influence of salinity on ancient vertebrate aquatic environments that may not be obvious from combined sedimentological and paleontological data alone.

ACKNOWLEDGMENTS

We thank S. Hasiotis and P. Zippi for identifying trace fossils and palynomorphs; funding and support from Bucknell University and Lycoming College; and P. Bourdon, C. Treaster, O. Goodchild, A. Elezier, J. Downs, and J. Sime for assistance with fieldwork and sample collection. We thank F. Thibon (LGL-TPE) for assistance with elementary analyses and E. Poulaillon (LGL-TPE) for help with sulfur isotope processing. S. Olive received funding from the European Union's Horizon 2020 research and innovation program under the Marie Sklodowska-Curie grant agreement No 101032456-TNT and from a Belspo FED-tWIN project from the Belgian Federal Government (Prf-2021-009-EAT). Finally, we thank the two anonymous reviewers and the associate editor Alessandro Zanazzi for their comments, which helped to improve the manuscript.

Author Contributions: J.G. S.O. and R.A. prepared geochemical samples. J.G., A.V.-L. and F.F. measured isotopic compositions on all samples. S.O. measured elemental content on all samples. Trop conceived the project and collected sedimentological observations. D.B. and T.D. collected paleontological observations. J.G., D.B., J.T, and T.D. made the figures and the Supplementary Material Item. All authors wrote the manuscript.

REFERENCES CITED

Blakey, R.C., Fielding, C.R., Frank, T.D. and Isbell, J.L., 2008. Gondwana paleogeography from assembly to breakup—A 500 my odyssey. *in* C.R. Fielding, T.D. Frank, and J.L. Isbell (eds.), Resolving the Late Paleozoic Ice Age in Time and Space: Geological Society of America Special Paper, v. 441, p. 1–28.

Broussard, D., Trop, J.M., Benowitz, J.A., Daeschler, E., Chamberlain, J., Chamberlain, R., 2018, Depositional setting, taphonomy and geochronology of new fossil sites in the Catskill Formation (Upper Devonian) of northern Pennsylvania, USA, including a new early tetrapod fossil: Palaeogeography, Palaeoclimatology, Palaeoecology, v. 511, p. 168–187.

Broussard, D., Treaster, C., Trop, J.M., Daeschler, E., Zippi, P., Vrazo, M., Rygel, M., 2020, Vertebrate taphonomy, paleontology, sedimentology, and palynology of a fossiliferous Late Devonian fluvial succession, Catskill Formation, north-central Pennsylvania, USA: Palaois, v. 35, p. 470–494.

Broussard, D.R., Burrow, C.J., Trop, J.M., Kennedy, S., Daeschler, E.B., and Zippi, P.A., 2022, First records of Ischnacanthiformes ("Acanthodii") from the Upper Devonian Catskill Formation in north-central Pennsylvania, USA: Journal of Vertebrate Paleontology, v. 42, p e2212009.

Byrne, H.M., Green, J.A.M., Balbus, S.A., and Ahlberg, P.E., 2020, Tides: A key environmental driver of osteichthyan evolution and the fish-tetrapod transition?: Proceedings of the Royal Society A, v. 476(2242), p. 20200355.

Carr, R.K., 1995, Opportunity knocked and no one was home: aspinothoracid arthrodires (Placodermi) from the Ohio Shale Formation (upper Devonian, North America): Geobios, v. 19, p. 81–83.

Carr, R.K., 2010. Paleoecology of *Dunkleosteus terrelli* (Placodermi: Arthrodira): Kirtlandia, v. 57, p. 36–45.

Carr, R.K., and Jackson, G.L., 2010, The vertebrate fauna of the Cleveland Member (Famennian) of the Ohio Shale, Chapter 5, *in* Hannibal, J.T., ed., Guide to the Geology and Paleontology of the Cleveland Member of the Ohio Shale, Ohio Geological Survey Guidebook 22.

Carpenter, D.K., Falcon-Lang, H.J., Benton, M.J., and Grey, M., 2015, Early Pennsylvanian (Langsettian) fish assemblages from the Joggins Formation, Canada, and their implications for palaeoecology and palaeogeography. Palaeontology, v. 58, p. 661–690.

427 Castle, J.W., 2000, Recognition of facies, bounding surfaces, and stratigraphic patterns in foreland-ramp
428 successions: An example from the Upper Devonian, Appalachian basin, USA: Journal of Sedimentary
429 Research, v. 70, p. 896–912.

430

431 Chen, B., Ma, X., Mills, B.J., Qie, W., Joachimski, M.M., Shen, S., Wang, C., Xu, H., and Wang, X., 2021, Devonian
432 paleoclimate and its drivers: A reassessment based on a new conodont $\delta^{18}O$ record from South China:
433 Earth-Science Reviews, v. 222, p. 103814.

434 Chevrinais, M., Jacquet, C. and Cloutier, R. 2017. Early establishment of vertebrate tropic interactions: food
435 web structure in Middle to Late Devonian fish assemblages with exceptional fossilization. Bulletin of
436 Geosciences, 92, 491–510.

437 Clack, J.A., 2002, Gaining Ground: the Origin and Evolution of Tetrapods: Indiana University Press, Bloomington,
438 IN, 544 p.

439 Cloern, J.E., Jassby, A.D., Schraga, T.S., Nejad, E., and Martin, C., 2017, Ecosystem variability along the estuarine
440 salinity gradient: Examples from long-term study of San Francisco Bay: Limnology and Oceanography,
441 v. 62, p. S272–S291.

442 Cloutier, R., Proust, J.N., and Tessier, B., 2011, The Miguasha Fossil-Fish-Lagerstätte: a consequence of the
443 Devonian land–sea interactions: Palaeobiodiversity and Palaeoenvironments, v. 91, p.293–323.

444 Colombano, D.D., Manfree, A.D., Teejay, A.O., Durand, J.R., and Moyle, P.B., 2020, Estuarine-terrestrial habitat
445 gradients enhance nursery function for resident and transient fishes in the San Francisco Estuary:
446 Marine Ecology Progress Series, v. 637, p. 141–157.

447 Community Bureau of Reference, 1982, Certified reference material certificate of analyses for BCR No. 32.
448 Commission of the European Communities, Report No. 541.

449 Craig, H. and Gordon, L. I., 1965, Deuterium and oxygen variations in the ocean and the marine atmosphere *in*
450 *Stable Isotopes in Oceanographic Studies and Paleotemperatures* (ed. Tongiorgo, E.) p. 9–130.

Cressler III, W.L., Daeschler, E.B., Slingerland, R., and Peterson, D.A., 2010, Terrestrialization in the Late Devonian: a palaeoecological overview of the Red Hill site, Pennsylvania, USA: Geological Society, London, Special Publications, v. 339, p. 111–128.

Croisetiere, L., Hare, L., Tessier, A., and Cabana, G., 2009, Sulphur stable isotopes can distinguish trophic dependence on sediments and plankton in boreal lakes: Freshwater Biology, v. 54, p. 1006–1015.

Crowson R.A., Showers W.J., Wright E.K., Hoering T.C., 1991, Preparation of phosphate samples for oxygen isotope analysis: Analytical Chemistry, v. 63, p. 2397–2400.

Daeschler, E.B., Clack, J.A., and Shubin, N.H., 2009, Late Devonian tetrapod remains from Red Hill, Pennsylvania, USA: how much diversity?: Acta Zoologica, v. 90, p. 306–317.

Daeschler, E.B., and Cressler, W.L., III, 2011, Late Devonian paleontology and paleoenvironments at Red Hill and other fossil sites in the Catskill Formation of north-central Pennsylvania, *in* Ruffolo, R.M. and Ciampaglio, C.N. eds., From the Shield to the Sea, Geological Society of America, v. 20, p. 0, doi:10.1130/2011.0020(01).

Dansgaard, W., 1964, Stable isotopes in precipitation: Tellus, v. 16, p. 436–468.

De Brabandere, L., Catalano, M.J., Frazer, T.K., and Allen, M.S., 2009, Stable isotope evidence of ontogenetic changes in the diet of gizzard shad Dorosoma cepedianum: Journal of Fish Biology, v. 74, p. 105–119.

Doubleday, Z.A., Cliff, J., Izzo, C., and Gillanders, B.M., 2018, Untapping the potential of sulfur isotope analysis in biominerals: Marine Ecology Progress Series, v. 598, p. 159–166.

Downs, J.P., Barbosa, J., and Daeschler, E.B., 2021, A new species of *Eusthenodon* (Sarcopterygii, Tristichopteridae) from the Upper Devonian (Famennian) of Pennsylvania, USA, and a review of *Eusthenodon* taxonomy: Journal of Vertebrate Paleontology, v. 41, p. e1976197.

Dubé, M.G., Benoy, G.A., Blenkinsopp, S., Ferone, J.-M., Brua, R.B., and Wassenaar, L.I., 2005, Application of multi-stable isotope (13C, 15N, 34S, 37Cl) assays to assess spatial separation of fish (longnose sucker

474 Catostomus catostomus) in an area receiving complex effluents: Water Quality Research Journal of
475 Canada, v. 40, p. 275–287.

476 Every, S.L., Pethybridge, H.R., Fulton, C.J., Kyne, P.M., and Crook, D.A., 2017, Niche metrics suggest euryhaline
477 and coastal elasmobranchs provide trophic connections among marine and freshwater biomes in
478 northern Australia: Marine Ecology Progress Series, v. 565, p. 181–196.

479 Fourel, F., Martineau, F., Lécuyer, C., Kupka, H.J., Lange, L., Ojeimi, C. and Seed, M., 2011, $^{18}O/^{16}O$ ratio
480 measurements of inorganic and organic materials by elemental analysis–pyrolysis–isotope ratio mass
481 spectrometry continuous-flow techniques: Rapid Communications in Mass Spectrometry, v. 25, p.
482 2691–2696.

483 Fourel F., Martineau F., Seris M., and Lécuyer C., 2015, Measurement of $^{34}S/^{32}S$ ratios of NBS 120c and BCR 32
484 phosphorites using purge and trap EA-IRMS technology: Geostandards and Geoanalytical Research, v.
485 39, p. 47–53.

486 Fry, B., 2002a, Conservative mixing of stable isotopes across estuarine salinity gradients: a conceptual
487 framework for monitoring watershed influences on downstream fisheries production: Estuaries, v. 25,
488 p. 264–271.

489 Fry, B., 2002b, Stable isotopic indicators of habitat use by Mississippi River fish: Journal of the North American
490 Benthological Society, v. 21, p. 676–685.

491 Fry, B., and Chumchal, M.M., 2011, Sulfur stable isotope indicators of residency in estuarine fish: Limnology
492 and Oceanography, v. 56, p. 1563–1576.

493 Geawhari, M.A., Huff, L., Mhammdi, N., Trakadas, A., and Ammar, A., 2014, Spatial-temporal distribution of
494 salinity and temperature in the Oued Loukkos estuary, Morocco: using vertical salinity gradient for
495 estuary classification: SpringerPlus, v. 3, p. 1–9.

496 Gess, R.W., and Whitfield, A.K., 2020, Estuarine fish and tetrapod evolution: insights from a Late Devonian
497 (Famennian) Gondwanan estuarine lake and a southern African Holocene equivalent: Biological
498 Reviews, v. 95(4), p. 865–888.

Gilleaudeau, G.J., Algeo, T.J., Lyons, T.W., Bates, S., and Anbar, A.D., 2021, Novel watermass reconstruction in the Early Mississippian Appalachian Seaway based on integrated proxy records of redox and salinity: Earth and Planetary Science Letters, v. 558, 116746.

Godebout, L., Trudel, M., Irvine, J.R., Wood, C.C., Grove, M.J., Schmitt, A.K., and McKeegan, K.D., 2010, Sulfur isotopes in otoliths allow discrimination of anadromous and non-anadromous ecotypes of sockeye salmon (Oncorhynchus nerka): Environmental Biology of Fishes, v. 89, p. 521–532.

Godebout, L., Wood, C.C., Withler, R.E., Latham, S., Nelson, R.J., Wetzel, L., Barnett-Johnson, R., Grove, M.J., Schmitt, A.K., and McKeegan, K.D., 2011, Sockeye salmon (*Oncorhynchus nerka*) return after an absence of nearly 90 years: a case of reversion to anadromy: Canadian Journal of Fisheries and Aquatic Sciences, v. 68, p. 1590–1602.

Goedert, J., Fourel, F., Amiot, R., Simon, L., and Lécuyer, C., 2016, High-precision $^{34}S/^{32}S$ measurements in vertebrate bioapatites using purge-and-trap EA-IRMS technology: Rapid Communications in Mass Spectrometry, v. 30, p. 2002–2008.

Goedert, J., Lécuyer, C., Amiot, R., Arnaud-Godet, F., Wang, X., Cui, L., Cuny, G., Douay, G., Fourel, F., Panczer, G., and Simon, L., 2018, Euryhaline ecology of early tetrapods revealed by stable isotopes: Nature, v. 558, p. 68–72.

Goedert, J., Amiot, R., Berthet, D., Fourel, F., Simon, L., and Lécuyer, C., 2020, Combined oxygen and sulphur isotope analysis—a new tool to unravel vertebrate (paleo)-ecology: The Science of Nature, v. 107, p. 1–9.

Goedert, J., Amiot, R., Anquetin, J., Séon, N., Bourgeais, R., Bailly, G., Fourel, F., Simon, L., Li, C., Wang, W., and Lécuyer, C. 2023, Multi-isotopic analysis reveals the early stem turtle *Odontochelys* as a nearshore herbivorous forager: Frontiers in Ecology and Evolution, v. 11.

Gogáin, A., Falcon-Lang, H.J., Carpenter, D.K., Miller, R.F., Benton, M.J., Pufahl, P.K., Ruta, M., Davies, T.G., Hinds, S.J., and Stimson, M.R., 2016, Fish and tetrapod communities across a marine to brackish salinity gradient in the Pennsylvanian (early Moscovian) Minto Formation of New Brunswick, Canada, and their palaeoecological and palaeogeographical implications: Palaeontology, v. 59, p. 689–724.

525 Golonka, J., 2020, Late Devonian paleogeography in the framework of global plate tectonics: Global and
526 Planetary Change, v. 186, p. 103129.
527 Halas S, Szaran J., 2001, Improved thermal decomposition of sulfates to SO_2 and mass spectrometric
528 determination of $\delta^{34}S$ of IAEA SO-5, IAEA SO-6 and NBS-127 sulfate standards: Rapid Communicaitons
529 in Mass Spectrometry, v. 15, p. 1618–1620.

530 Hesslein, R.H., Capel, M.J., Fox, D.E., and Hallard, K.A., 1991, Stable isotopes of sulfur, carbon, and nitrogen as
531 indicators of trophic level and fish migration in the lower Mackenzie River basin, Canada: Canadian
532 Journal of Fisheries and Aquatic Sciences, v. 48, p. 2258–2265.

533 Joachimski, M.M., Breisig, S., Buggisch, W., Talent, J.A., Mawson, R., Gereke, M., Morrow, J.R., Day, J., and
534 Weddige, K., 2009, Devonian climate and reef evolution: Insights from oxygen isotopes in apatite:
535 Earth and Planetary Science Letters, v. 284, p. 599–609, https://doi.org/10.1016/j.epsl.2009.05.028.

536 Kampschulte, A., and Strauss, H., 2004, The sulfur isotopic evolution of Phanerozoic seawater based on the
537 analysis of structurally substituted sulfate in carbonates: Chemical Geology, v. 204, p. 255–286.

538 Keenan, S.W., 2016, From bone to fossil: A review of the diagenesis of bioapatite: American Mineralogist, v.
539 101, p. 1943–1951.

540 Keenan, S.W., and Engel, A.S., 2017, Early diagenesis and recrystallization of bone: Geochimica et
541 Cosmochimica Acta, v. 196, p. 209–223.

542 Keenan, S.W., Engel, A.S., Roy, A., and Bovenkamp-Langlois, G.L., 2015, Evaluating the consequences of
543 diagenesis and fossilization on bioapatite lattice structure and composition: Chemical Geology, v. 413,
544 p. 18–27.

545 Koeppenkastrop, D., and Eric, H., 1992, Sorption of rare-earth elements from seawater onto synthetic mineral
546 particles: An experimental approach: Chemical geology, v. 95, p. 251–263.

547 Lécuyer, C., Fourel, F., Martineau, F., Amiot, R., Bernard, A., Daux, V., Escarguel, G. and Morrison, J., 2007, High-
548 precision determination of $^{18}O/^{16}O$ ratios of silver phosphate by EA-pyrolysis-IRMS continuous flow
549 technique. Journal of Mass Spectrometry v. 42, p. 36–41.

Lécuyer C., Fourel F., Seris M., Amiot R., Goedert J., Simon L. 2019. Synthesis of in-house produced calibrated silver phosphate with a large range of oxygen isotope compositions. Geostandards and Geoanalytical Research

Lécuyer, C., Grandjean, P., O'Neil, J.R., Cappetta, H. and Martineau, F., 1993, Thermal excursions in the ocean at the Cretaceous—Tertiary boundary (northern Morocco): δ18O record of phosphatic fish debris: Palaeogeography, Palaeoclimatology, Palaeoecology, v. 105, p. 235–243.

Lécuyer, C., Grandjean, P., and Sheppard, S.M.F., 1999, Oxygen isotope exchange between dissolved phosphate and water at temperatures ≤135°C: inorganic versus biological fractionations: Geochimica et Cosmochimica Acta, v. 63, p. 855–862.

Martin, J.E., Tacail, T., Cerling, T.E., and Balter, V., 2018, Calcium isotopes in enamel of modern and Plio-Pleistocene East African mammals: Earth and Planetary Science Letters, v. 503, p. 227–235.

Nehlich, O., Barrett, J.H., and Richards, M.P., 2013, Spatial variability in sulphur isotope values of archaeological and modern cod (Gadus morhua): Rapid Communications in Mass Spectrometry, v. 27, p. 2255–2262.

Nehlich, O., 2015, The application of sulphur isotope analyses in archaeological research: A review. Earth-Science Reviews 142:1–17.

Oest, C., 2015, Paleopedology and fluvial sedimentology of the Upper Devonian Catskill Formation of Pennsylvania: a test of the distributive fluvial system model, MS thesis, Temple University, Philadelphia, Pennsylvania, 105 p.

Olive, S., Ahlberg, P.E., Pernègre, V.N., Poty, É., Steurbaut, É., and Clément, G., 2016, New discoveries of tetrapods (ichthyostegid-like and whatcheeriid-like) in the Famennian (Late Devonian) localities of Strud and Becco (Belgium) (Z. Johanson, Ed.): Palaeontology, v. 59, p. 827–840.

Paytan, A., Yao, W., Faul, K.L., and Gray, E.T., 2020, Sulfur isotope stratigraphy, *in* Geologic Time Scale 2020, Elsevier, p. 259–278.

573 Peryt, T.M., Makhnach, A.A., Halas, S., Petrychenko, O.Y., Gulis, L.F., and Abravets, S.M., 2007, Sulfur isotopes
574 in anhydrites from the Upper Devonian Prypiac'and Dnipro-Donets Basins (Belarus and Ukraine):
575 Carbonates and Evaporites, v. 22, p. 43–54.

576 Peterson, B.J., Howarth, R.W., and Garritt, R.H., 1986, Sulfur and Carbon isotopes as tracers of salt-marsh
577 organic matter flow: Ecology, v. 67, p. 865–874.

578 Pizzochero, A.C., Michel, L.N., Chenery, S.R., McCarthy, I.D., Vianna, M., Malm, O., Lepoint, G., Das, K., and
579 Dorneles, P.R., 2018, Use of multielement stable isotope ratios to investigate ontogenetic movements
580 of Micropogonias furnieri in a tropical Brazilian estuary: Canadian Journal of Fisheries and Aquatic
581 Sciences, v. 75, p. 977–986.

582 Rountree, R.A., and Able, K.W., 2007, Spatial and temporal habitat use patterns for salt marsh nekton:
583 implications for ecological functions: Aquatic Ecology, v. 41, p. 25–45.

584 Rozanski K, Araguás-Araguás L, and Gonfiantini R., 1993, Isotopic patterns in modern global precipitation.
585 Climate change in continental isotopic records, p. 1–36.

586 Reynard, B., Lécuyer, C., and Grandjean, P., 1999, Crystal-chemical controls on rare-earth element
587 concentrations in fossil biogenic apatites and implications for paleoenvironmental reconstructions:
588 Chemical Geology, v. 155, p. 233–241.

589 Sak, P.B., McQuarrie, N., Oliver, B.P., Lavdovsky, N. and Jackson, M.S., 2012, Unraveling the central Appalachian
590 fold-thrust belt, Pennsylvania: The power of sequentially restored balanced cross sections for a blind
591 fold-thrust belt: *Geosphere*, v. *8*, p. 685–702.

592 Sallan, L., Friedman, M., Sansom, R.S., Bird, C.M., and Sansom, I.J., 2018, The nearshore cradle of early
593 vertebrate diversification: Science, v. 362, p. 460–464.

594 Schultz, E.T., and McCormick, S.D., 2012, Euryhalinity in an evolutionary context: Fish physiology, v. 32, p. 477–
595 533.

596 Shemesh, A., Kolodny, Y., and Luz, B., 1983, Oxygen isotope variations in phosphate of biogenic apatites, II.
597 Phosphorite rocks: Earth and Planetary Science Letters, v. 64, p. 405–416.

598 Sim, M.S., Ono, S., and Hurtgen, M.T., 2015, Sulfur isotope evidence for low and fluctuating sulfate levels in the
599 Late Devonian ocean and the potential link with the mass extinction event: Earth and Planetary
600 Science Letters, v. 419, p. 52–62.

601 Slane, D.C., and Rygel, M.C., 2009, Marginal-marine facies of the Catskill Formation (Upper Devonian), Tioga
602 County, Pennsylvania. In Geological Society of America Annual Meeting.

603 Sponheimer, M., and Lee-Thorp, J.A., 2006, Enamel diagenesis at South African Australopith sites: Implications
604 for paleoecological reconstruction with trace elements: Geochimica et Cosmochimica Acta, v. 70, p.
605 1644–1654.

606 Trembaczowski, A., 2011, Use of sulphur and carbon stable-isotope composition of fish scales and muscles to
607 identify the origin of fish: Mineralogia, v. 42, p. 33.

608 Trotter, J.A., Barnes, C.R., and McCracken, A.D., 2016, Rare earth elements in conodont apatite: Seawater or
609 pore-water signatures?: Palaeogeography, Palaeoclimatology, Palaeoecology, v. 462, p. 92–100.

610 Trueman, C.N., and Tuross, N., 2002, Trace elements in recent and fossil bone apatite: Reviews in mineralogy
611 and geochemistry, v. 48, p. 489–521.

612 Veale, L., Tweedley, J.R., Clarke, K.R., Hallett, C.S., and Potter, I.C., 2014, Characteristics of the ichthyofauna of a
613 temperate microtidal estuary with a reverse salinity gradient, including inter-decadal comparisons:
614 Journal of Fish Biology, v. 85, p. 1320–1354.

615 Weber, P.K., Hutcheon, I.D., McKeegan, K.D., and Ingram, B.L., 2002, Otolith sulfur isotope method to
616 reconstruct salmon (Oncorhynchus tshawytscha) life history: Canadian Journal of Fisheries and Aquatic
617 Sciences, v. 59, p. 587–591.

618 Xia, X., Guo, W., Tan, S., and Liu, H., 2017, Synechococcus assemblages across the salinity gradient in a salt
619 wedge estuary: Frontiers in microbiology, v. 8, p. 1254.

Young, M.J., Feyrer, F.V., Colombano, D.D., Louise Conrad, J., and Sih, A., 2018, Fish-habitat relationships along the estuarine gradient of the Sacramento-San Joaquin Delta, California: implications for habitat restoration: Estuaries and Coasts, v. 41, p. 2389–2409.

Zhang, G., Bai, J., Tebbe, C.C., Zhao, Q., Jia, J., Wang, W., Wang, X., and Yu, L., 2021, Salinity controls soil microbial community structure and function in coastal estuarine wetlands: Environmental Microbiology, v. 23, p. 1020–1037.

Zydlewski, J., and Wilkie, M.P., 2012, Freshwater to seawater transitions in migratory fishes, *in* Fish physiology, Elsevier, v. 32, p. 253–326.

FIGURE CAPTIONS

Figure 1 – A. Map showing Upper Devonian sedimentary strata in New York and Pennsylvania (yellow). Red rectangle highlights the geographic area containing sampled vertebrate fossil sites (yellow circles) and unsampled vertebrate fossils sites (gray circles). Adapted from Broussard et al. (2018). B. Stratigraphic chart showing maximum age range of sampled vertebrate sites based on palynology (SMI 1). C. Depositional setting of Late Devonian vertebrate fossil sites ca. 362 Ma. Area shown in C spans ~30°–35° S of the paleoequator (Golonka, 2020). Red rectangle corresponds to area shown in A and yellow circles are sampled vertebrate fossil sites also shown in A. D. Schematic depositional model for Catskill and Lock Haven formation strata in north-central Pennsylvania with sampled (red text) and unsampled (green text) fossil localities. Modified from Oest (2015) and Broussard et al. (2020). Green symbols indicate tetrapod occurrences at upstream sites (see text for references). Base paleogeography is from 2023 Colorado Plateau Geosystems Inc. Refer to SMI 1 and 2 for details on the fossil sites where isotope samples were collected.

Figure 2 – PAAS normalized REY diagrams for bioapatite and sediment samples from the Steam Valley, Blossburg, Tioga and Covington (Middle and South) localities on the upper part and $(La/Yb)_N$ vs $(La/Sm)_N$ and $(Sm/Yb)_N$ vs $(La/Sm)_N$ diagrams on the lower part. The sediment samples are shown as light pink in the REY diagrams and as stars in the ratio diagrams. The grey shaded area corresponds to the so-called "bell-shaped" zone that characterizes MREE enrichment due to substitution mechanisms with calcium during late diagenetic phases following the model of Reynard et al. (1999). For the Tioga locality the blue dots circled in bold represent the calculated values (using the apatite-water K_d partition coefficient determined by Koeppenkastrop and De Carlo 1992) for the pore waters from which the Devonian apatite samples from the Tioga locality would have acquired their REY (following Trotter et al., 2016).

Figure 3 – Stable sulfur isotope composition vs stable oxygen isotope composition of Late Devonian vertebrate bioapatite samples from different Pennsylvanian localities. Black horizontal dashed lines (positioned arbitrarily) delimit three main areas of aquatic environments characterized by contrasting salinities, based on $\delta^{34}S$ values.

Figure 4 – Stable sulfur isotope composition vs stable oxygen isotope composition of Late Devonian vertebrate bioapatite samples from Pennsylvania (this study) compared to those previously measured for East Greenland and China Late Devonian vertebrate samples (East Greenland and China data are from Goedert et al., 2018). Black horizontal dashed lines (positioned arbitrarily) delimit three main areas of aquatic environments characterized by contrasting salinities, based on $\delta^{34}S$ values.

[1]Supplemental Material. *SMI 1–16* Please visit https://doi.org/10.1130/XXXX to access the supplemental material, and contact editing@geosociety.org with any questions.

SUPPLEMENTAL MATERIAL ITEMS

SMI 1 Goedert et al. Devonian Sites. Table summarizing vertebrate fossil sites. For site details, refer to SMI-2-7, as well as Broussard et al. (2018, 2020, 2022).

SMI 2 Goedert et al. Locality Map. Geologic map showing vertebrate fossil sites. For site details, refer to SMI-1, 3, and 4 as well as Broussard et al. (2018, 2020).

SMI 3 Goedert et al. Vertebrate fossils. Photographs of representative vertebrate taxa from each vertebrate fossil site.

SMI 4 Goedert et al. Steam Valley Samples. Photographs of sampled vertebrate macrofossils from Steam Valley

SMI 5 Goedert et al. Blossburg Samples. Photographs of sampled vertebrate macrofossils from Blossburg

SMI 6 Goedert et al. Tioga Samples. Photographs of sampled vertebrate macrofossils from Tioga

SMI 7 Goedert et al. Covington Samples. Photographs of sampled vertebrate macrofossils from Covington

SMI 8 Goedert et al. Table summarizing isotopic data

SMI 9 Goedert et al. Table summarizing elemental data

SMI 10 Goedert et al. Table summarizing REY data

SMI 11 Goedert et al. Covington Macrofossils. Photographs showing key macrofossils of the sampled Covington site, which has not been published previously.

683 **SMI 12 Goedert et al. Covington Lithofacies.** Photographs showing key sedimentological features of

684 the sampled Covington site, which has not been published previously.

685 **SMI 13 Goedert et al. Covington Trace Fossil.** Photographs showing key ichnofossils of the sampled

686 Covington site, which has not been published previously.

687 **SMI 14 Goedert et al. Taphonomic variation.** Photographs of representative vertebrate fossils

688 demonstrating taphonomic variation

689 **SMI 15 Goedert et al. Preservation of original isotopic signal.**

690 **SMI 16 Goedert et al. Mann-Whitney pairwise**

Figure 1

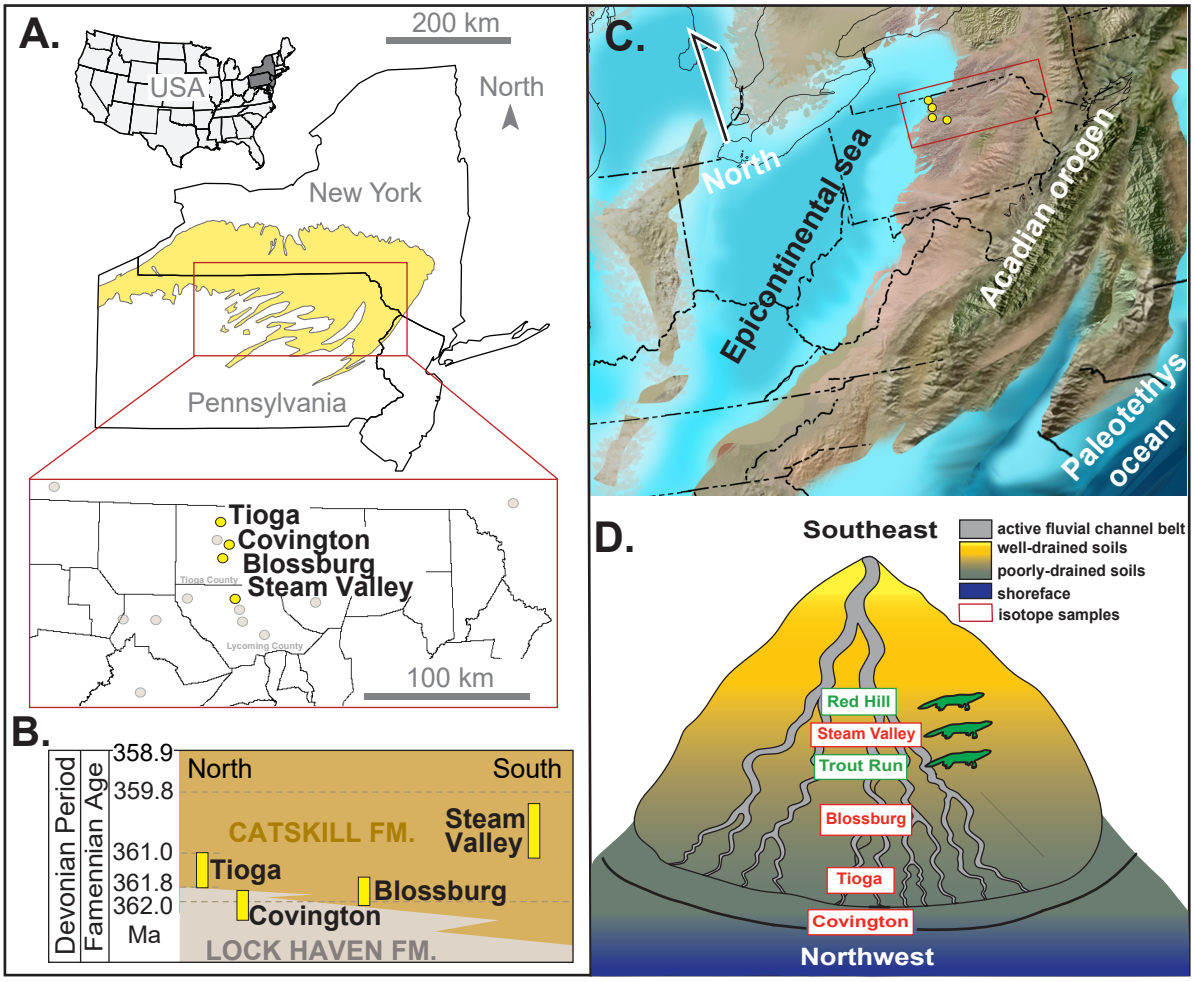

Goedert et al., Figure 1

Figure 2

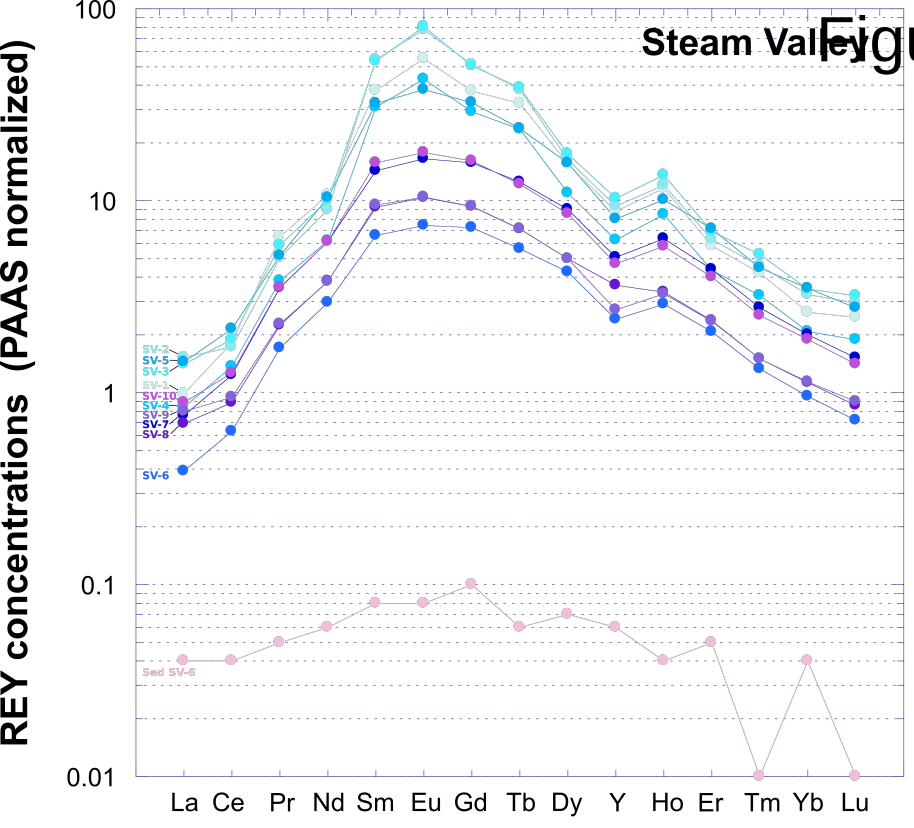
Steam Valley
REY concentrations (PAAS normalized)
100
10
1
0.1
0.01
SV-2
SV-5
SV-3
SV-1
SV-10
SV-4
SV-9
SV-7
SV-8
SV-6
Sed SV-6
La Ce Pr Nd Sm Eu Gd Tb Dy Y Ho Er Tm Yb Lu

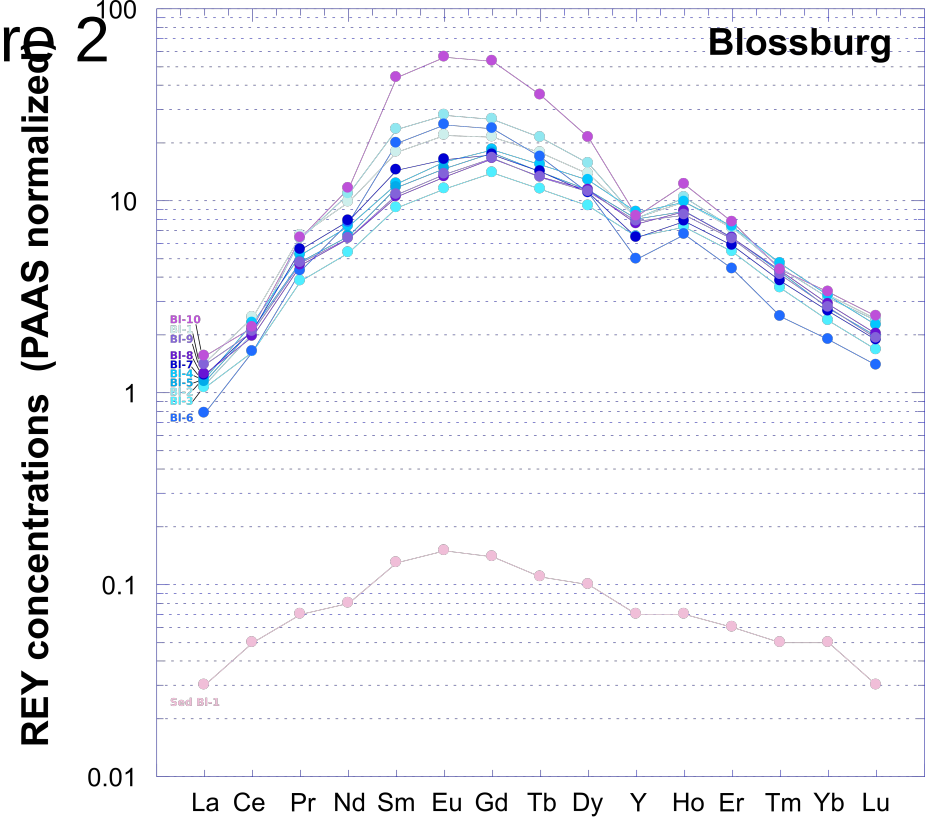
Blossburg
REY concentrations (PAAS normalized)
100
10
1
0.1
0.01
Bl-10
Bl-9
Bl-8
Bl-7
Bl-4
Bl-5
Bl-2
Bl-3
Bl-6
Sed Bl-1
La Ce Pr Nd Sm Eu Gd Tb Dy Y Ho Er Tm Yb Lu

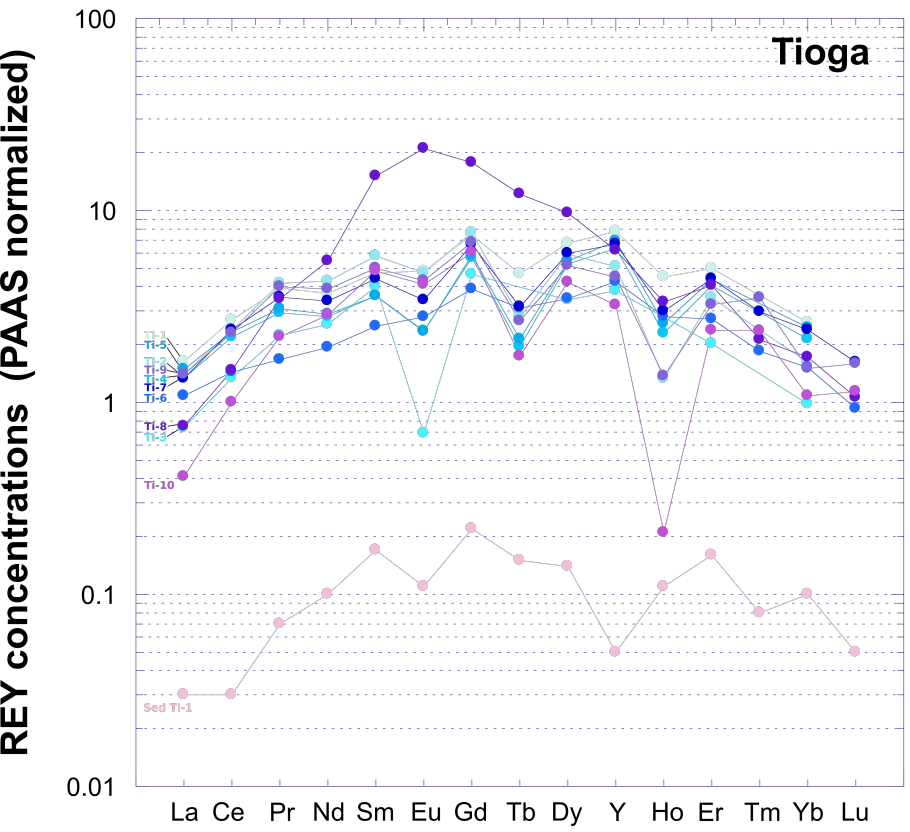
Tioga
REY concentrations (PAAS normalized)
100
10
1
0.1
0.01
Ti-1
Ti-5
Ti-9
Ti-4
Ti-7
Ti-6
Ti-8
Ti-3
Ti-10
Sed Ti-1
La Ce Pr Nd Sm Eu Gd Tb Dy Y Ho Er Tm Yb Lu

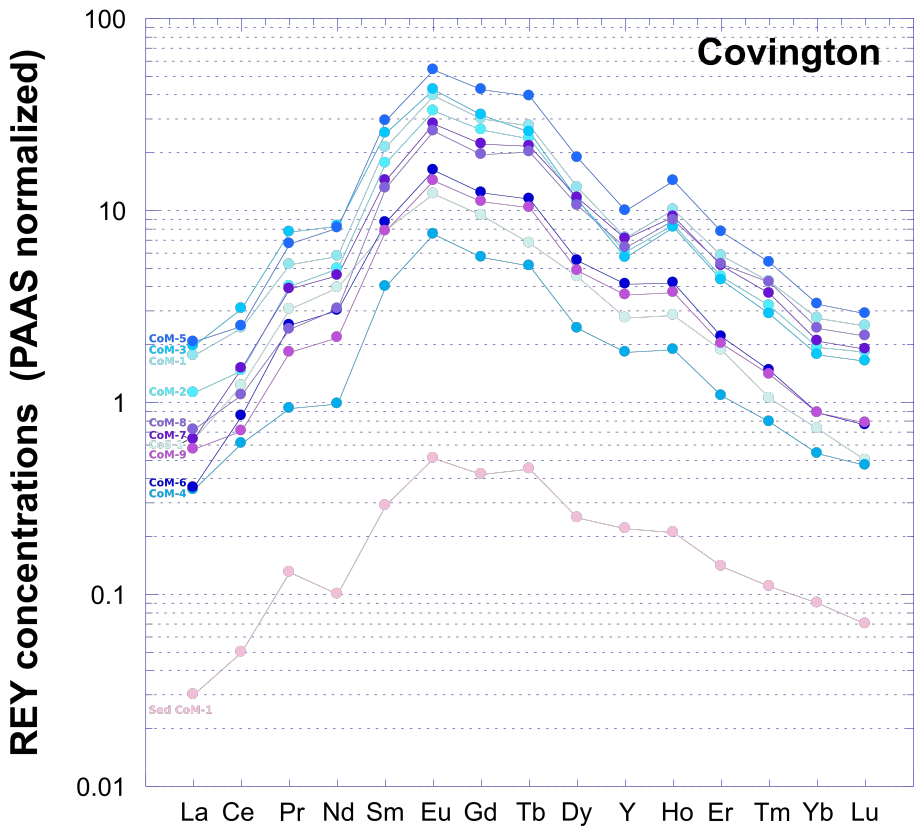
Covington
REY concentrations (PAAS normalized)
100
10
1
0.1
0.01
CoM-5
CoM-3
CoM-1
CoM-2
CoM-8
CoM-7
CoM-9
CoM-6
CoM-4
Sed CoM-1
La Ce Pr Nd Sm Eu Gd Tb Dy Y Ho Er Tm Yb Lu

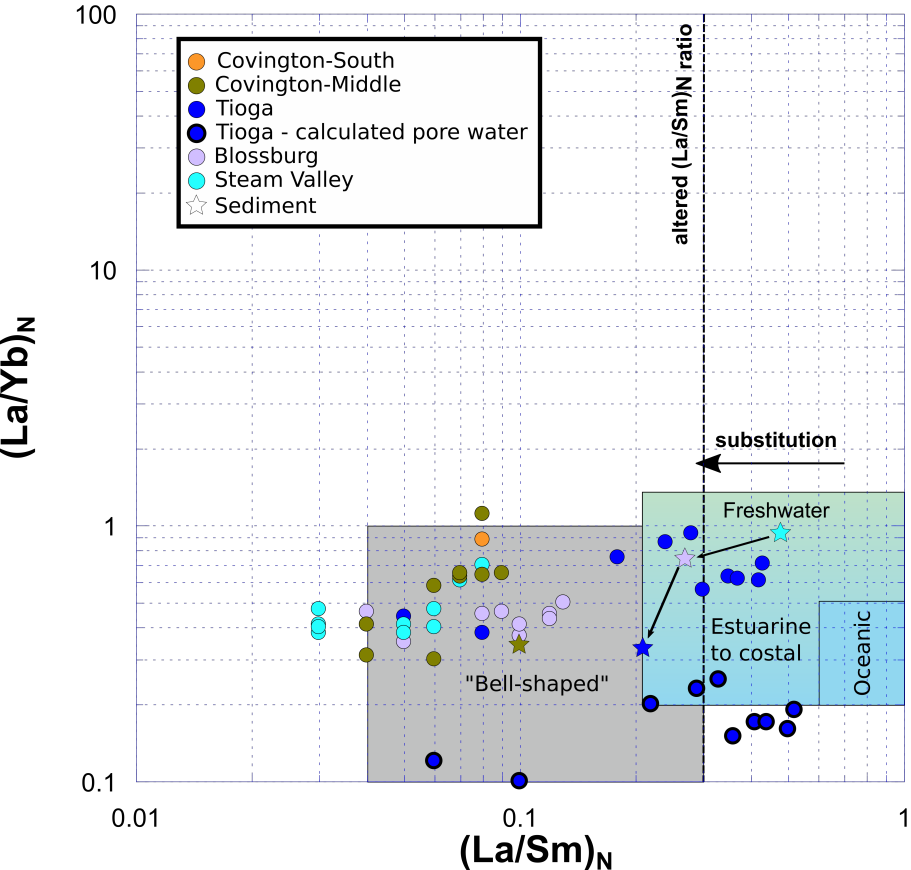
Covington-South
Covington-Middle
Tioga
Tioga - calculated pore water
Blossburg
Steam Valley
Sediment
altered (La/Sm)N ratio
substitution
Freshwater
Estuarine
to costal
Oceanic
"Bell-shaped"
(La/Yb)N
(La/Sm)N
100
10
1
0.1
0.01
0.1
1

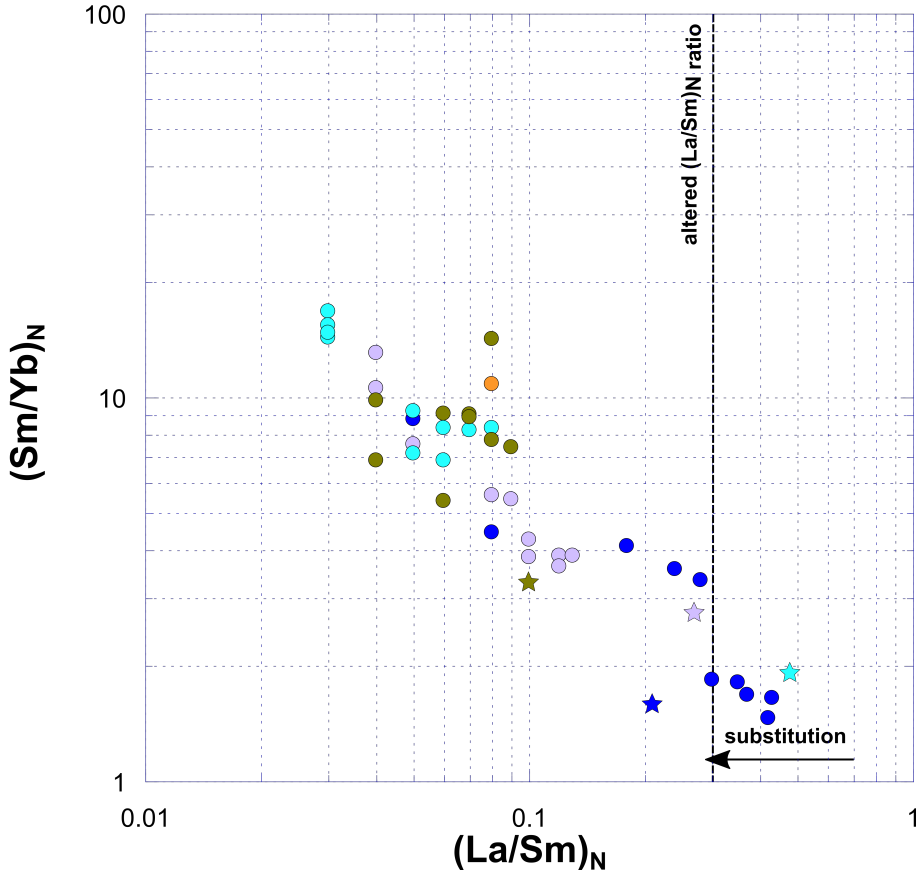
altered (La/Sm)N ratio
substitution
(Sm/Yb)N
(La/Sm)N
100
10
1
0.01
0.1
1

Figure 3

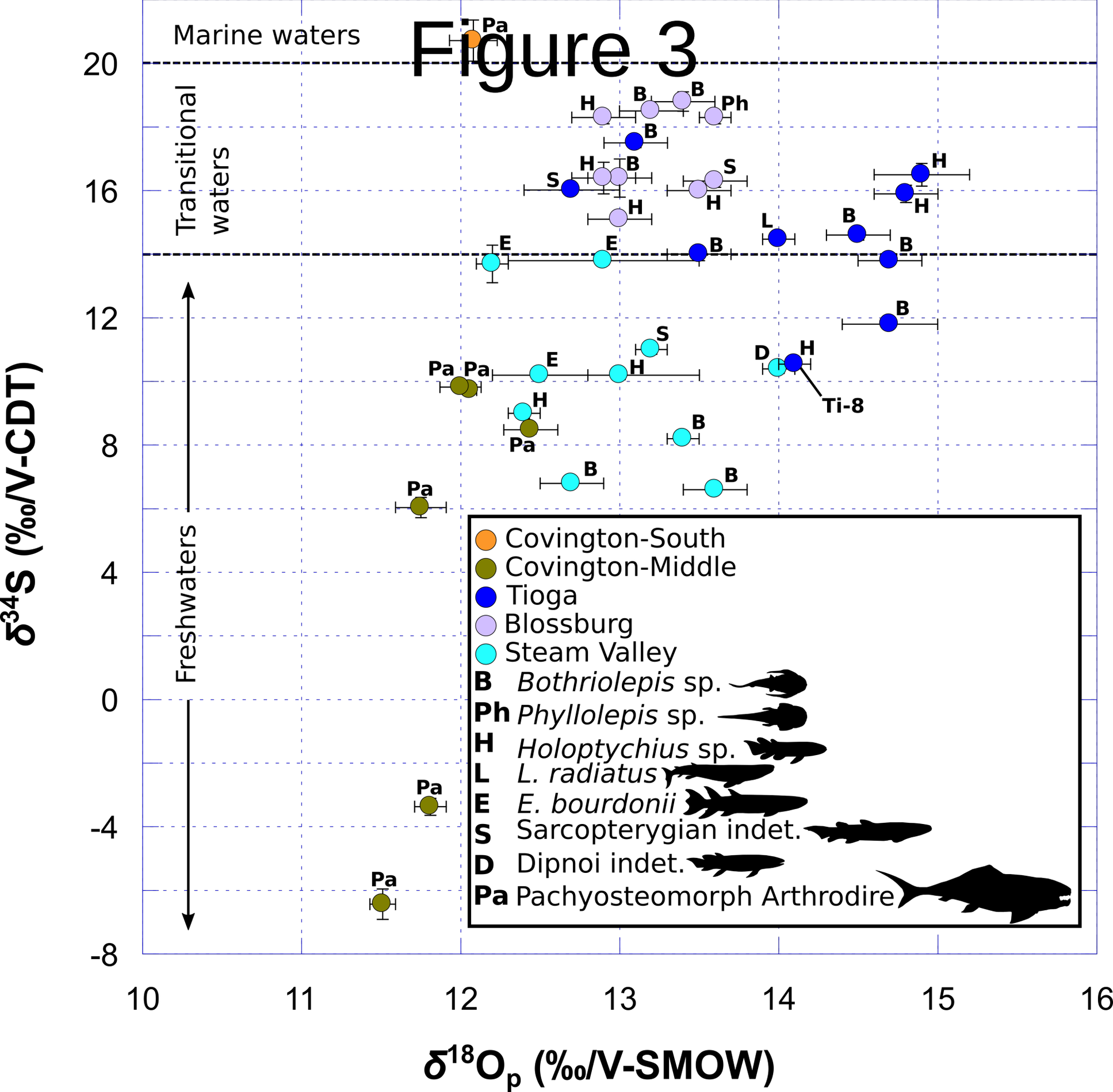
Marine waters
Transitional waters
Freshwaters
δ34S (‰/V-CDT)
δ18Op (‰/V-SMOW)
20
16
12
8
4
0
-4
-8
10
11
12
13
14
15
16
Ti-8
Covington-South
Covington-Middle
Tioga
Blossburg
Steam Valley
B Bothriolepis sp.
Ph Phyllolepis sp.
H Holoptychius sp.
L L. radiatus
E E. bourdonii
S Sarcopterygian indet.
D Dipnoi indet.
Pa Pachyosteomorph Arthrodire

Figure 4

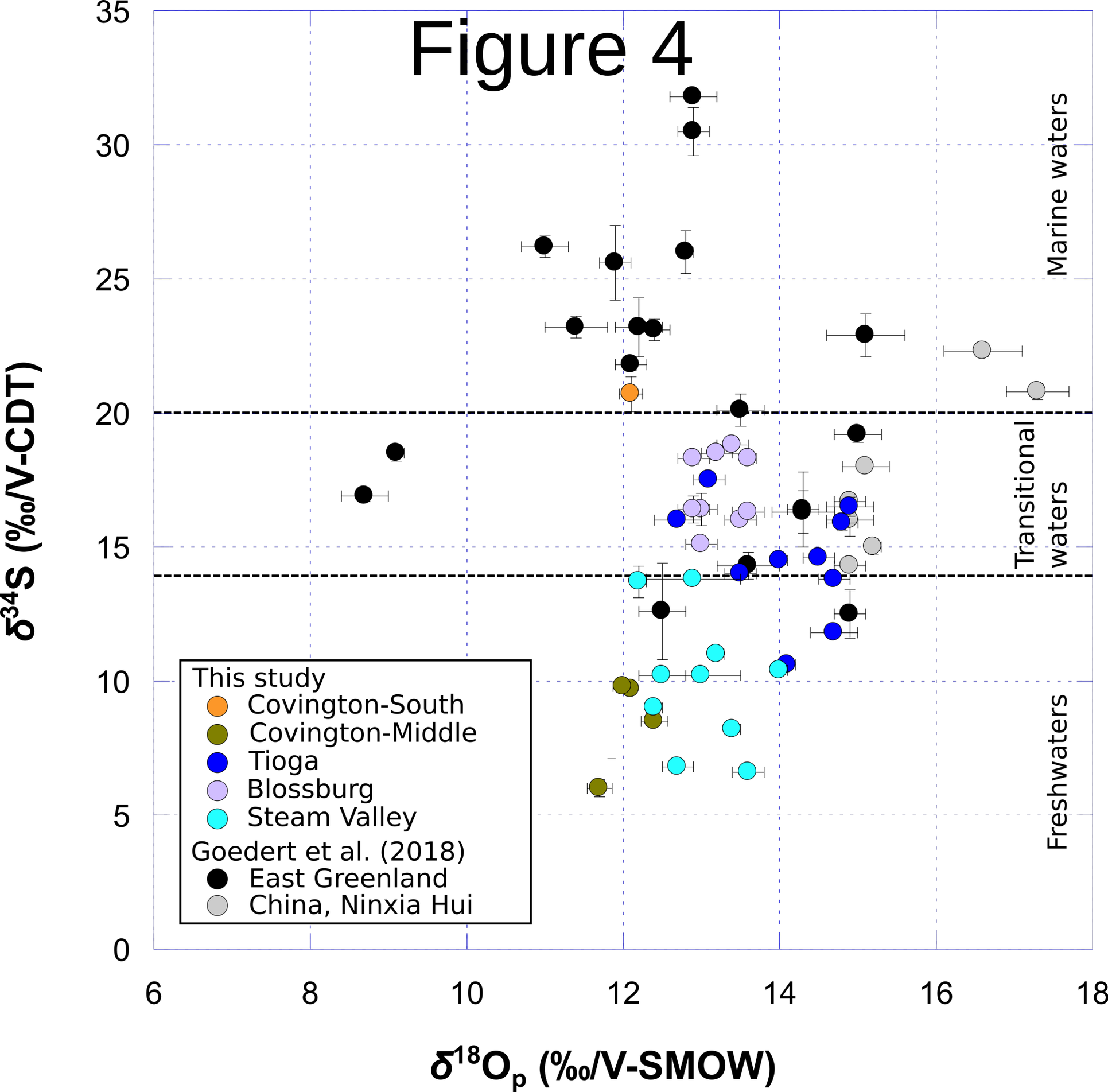
35
30
25
20
15
10
5
0
6
8
10
12
14
16
18
$\delta^{34}S$ (‰/V-CDT)
$\delta^{18}O_p$ (‰/V-SMOW)
Marine waters
Transitional waters
Freshwaters
This study
Covington-South
Covington-Middle
Tioga
Blossburg
Steam Valley
Goedert et al. (2018)
East Greenland
China, Ninxia Hui